Appl Phys B (2009) 96: 561–566
DOI 10.1007/s00340-009-3572-2

**Applied Physics B**
**Lasers and Optics**

# Modulated resonant versus pulsed resonant photoacoustics in trace gas detection

**R. Bartlome · M. Kaučikas · M.W. Sigrist**

Received: 2 February 2009 / Revised version: 28 April 2009 / Published online: 15 May 2009


**Abstract** Modulated resonant photoacoustics is a sensitive technique widely used for trace gas sensing. Generally, a continuous-wave laser is modulated at a frequency corresponding to an acoustic resonance of a photoacoustic cell. Another mode of operation—which we propose to call the pulsed resonant mode—consists in matching the frequency repetition rate of a pulsed laser to an acoustic resonance of the cell. We present a theoretical model to compare the performance of these two configurations. For a given average power of the incoming light inside the cell, the pulsed resonant mode of operation (nanosecond pulses or shorter) produces $\pi/2$ times higher photoacoustic signals than the modulated resonant scheme (the latter is optimized for a 50% duty cycle). This result agrees with experiments during which both cases were investigated at 532 nm using the same photoacoustic cell containing trace concentrations of $NO_2$.

**PACS** 82.80.Kq · 43.35.Ud · 07.07.Df

## 1 Introduction

Photoacoustic (PA) spectroscopy is a well-established technique that is often applied to detect trace concentrations of gases [1–3]. A PA cell can either be operated in a *modulated resonant* mode or in a *single-pulse* mode,[1] whereby the light excitation is a modulated continuous beam of light or a single short pulse, respectively. Both modes of operation have been extensively studied in literature [4–6]. Whereas in the modulated resonant case the modulation frequency is matched to an acoustic resonance of the PA cell, a broadband short pulse excites all acoustic modes at once. Another mode of operation—which we propose to call the *pulsed resonant* mode—consists in matching the pulse repetition rate of a pulsed source to an acoustic resonance of the PA cell. To the best of our knowledge, this third case has not been treated theoretically yet. On a few occasions, it has been applied as an alternative to continuous-wave (cw) lasers [7–9]. In this work, we compare the modulated resonant mode to the pulsed resonant mode under similar experimental conditions such as the wavelength, the average power or the diameter of the laser beam. Furthermore, we develop a theoretical comparison of both cases and conduct experiments using the same PA cell and absorbing species. For comparison purposes, we chose $NO_2$, for it strongly absorbs at 532 nm where both cw and pulsed laser sources are available. Furthermore, $NO_2$ is a pollutant of current interest that plays an important role in atmospheric chemistry [8, 10, 11].

## 2 Theory

### 2.1 Fourier series expansion of the PA signal

We derive a theoretical expression of the PA signal and compare the modulated resonant case with the pulsed resonant

R. Bartlome (✉) · M.W. Sigrist
Institute for Quantum Electronics, ETH Zurich,
Schafmattstrasse 16, 8093 Zurich, Switzerland
e-mail: richard.bartlome@alumni.ethz.ch

M.W. Sigrist
e-mail: sigrist@iqe.phys.ethz.ch

M. Kaučikas
Institute of Physics, Savanoriu 231, 2300 Vilnius, Lithuania

[1] In the literature—unlike in this work—single-pulse photoacoustics is sometimes referred to as pulsed resonant photoacoustics.

case. Let us assume that a beam of light is propagating parallel to the axis of a lossless cylindrical resonator. The dependence of the sound pressure $p$ on position $\mathbf{x}$ and time $t$ is given by the wave equation

$$\frac{\partial^2 p(\mathbf{x},t)}{\partial t^2} - c^2\nabla^2 p(\mathbf{x},t) = (\gamma-1)\frac{\partial H(\mathbf{x},t)}{\partial t}, \tag{1}$$

where $c$, $\gamma$, and $H$ are the sound velocity, the adiabatic coefficient of the gas, and the heat density deposited in the gas by light absorption, respectively. The sound pressure can be expanded into orthogonal resonator modes $p_n(\mathbf{x})$ as follows [1, 4]:

$$\begin{aligned} p(\mathbf{x},t) &= C_0(t) + \sum_{n=1}^{\infty} C_n(t)\,p_n(\mathbf{x}) \\ &= \sum_{m=-\infty}^{\infty} A_{0,m}e^{im\omega_0 t} + \sum_{n,m} A_{n,m}e^{im\omega_0 t}\,p_n(\mathbf{x}), \end{aligned} \tag{2}$$

whereby the eigenmode amplitudes $C_0(t)$ and $C_n(t)$ were further expanded into their Fourier series. The resonator eigenmodes $p_n(\mathbf{x},t)$ are solutions of the homogeneous wave equation,

$$\frac{\partial^2 p_n(\mathbf{x},t)}{\partial t^2} - c^2\nabla^2 p_n(\mathbf{x},t) = 0. \tag{3}$$

The solutions of (3) can be written as

$$p_n(\mathbf{x},t) = p_n(\mathbf{x})e^{i\omega_n t}, \tag{4}$$

where $\omega_n$ is the $n$-th eigenfrequency of the resonator. The heat source may also be expanded into a Fourier series as follows:

$$H(\mathbf{x},t) = H(\mathbf{x})H(t) = H(\mathbf{x})\sum_{m=-\infty}^{\infty} A_m^H e^{im\omega_0 t}. \tag{5}$$

Insertion of (4) into (3) leads to the following expression:

$$c^2\nabla^2 p_n(\mathbf{x}) = e^{-i\omega_n t}\,p_n(\mathbf{x})\frac{\partial^2 e^{i\omega_n t}}{\partial t^2} = -p_n(\mathbf{x})\omega_n^2. \tag{6}$$

We assume that the modulation frequency is tuned to the fundamental frequency of the resonator, i.e. $\omega_0 = \omega_1$, and that the PA signal is detected at this frequency. Therefore, only the cases where $|m| = 1$ are considered. The following expression can be derived by inserting (2), (5), and (6) into the wave equation (1), and equating coefficients of $e^{im\omega_0 t}$ and $e^{-im\omega_0 t}$:

$$\begin{aligned} &-\omega_0^2 A_{0,\pm1} + \sum_{n=1}^{\infty}\left(\omega_n^2 - \omega_0^2\right)A_{n,\pm1}\,p_n(\mathbf{x}) \\ &\quad = \pm i\omega_0(\gamma-1)H(\mathbf{x})A_{\pm1}^H. \end{aligned} \tag{7}$$

The Fourier coefficients $A_{n,\pm1}$ can be determined by multiplying (7) by $p_n(\mathbf{x})$ and integrating over the volume of the resonator $V$. Taking into account the fact that the value of the volume integral of all $p_n$ eigenmodes is zero [4], $A_{n,\pm1}$ can be expressed as

$$A_{n,\pm1} = \frac{\pm i\omega_0(\gamma-1)A_{\pm1}^H f_n}{\omega_n^2 - \omega_0^2}, \tag{8}$$

where the overlap integral $f_n$ is given by

$$f_n = \frac{\int_V H(\mathbf{x})p_n(\mathbf{x})\,dV}{\int_V p_n^2(\mathbf{x})\,dV}. \tag{9}$$

### 2.2 Heat source model

An expression of the Fourier coefficients $A_{\pm1}^H$ is derived for the modulated resonant and the pulsed resonant cases. The light source may either be a pulsed laser or a modulated cw laser (square pulse). Both light sources have an emission frequency $\nu$ and a pulse repetition rate $f$ given by $f = 1/T$, where $T$ is the pulse period ($T = 2\pi/\omega_0$). The pulse energy and the pulse duration are $E$ and $\tau_p$, respectively. The beam diameter change is negligible over the resonator length. The normalized beam profile $g(r)$ only depends on the radial position $r$ as it is assumed to be symmetrical around the axis of the beam:

$$\int 2\pi\, r\, g(r)\,dr = 1. \tag{10}$$

If $h$ is the Planck constant, the photon flux $\Phi(r,t)$ is given by

$$\Phi(r,t) = \frac{E}{h\nu}g(r)\Phi(t), \tag{11}$$

where the integration of $\Phi(t)$ over the duration of one pulse is written as

$$\int_{\text{pulse}} \Phi(t)\,dt = 1. \tag{12}$$

We assume that we have a two level system where the absorption cross section is $\sigma$ and the population densities of the lower and upper states are $N_0$ and $N_1$, respectively. Around atmospheric pressure, excited states decay with a characteristic time constant $\tau_{V-T}$ by means of collisional deactivation. If the light absorption is small ($N_0 \gg N_1$) as found in trace gas analyses, we can write [1]

$$H(r,t) = \frac{h\nu N_1(r,t)}{\tau_{V-T}}, \tag{13}$$

$$\frac{dN_1(r,t)}{dt} = N_0\sigma\,\Phi(r,t) - \frac{N_1(r,t)}{\tau_{V-T}}. \tag{14}$$

#### 2.2.1 Modulated resonant case

In the modulated resonant case $\tau_p \gg \tau_{V-T}$ [1]. Shortly after the start of the square pulse, the steady state $dN_1/dt = 0$ is reached. After the end of the pulse, $N_1(t)$ rapidly decays to zero. Thus $N_1(r,t)$ can be approximated by a square function, the amplitude of which is according to (11), (12), and (14)

$$N_1(r) = N_0\sigma \frac{E}{h\nu} g(r) \frac{\tau_{V-T}}{\tau_p}. \tag{15}$$

With (5), (13), and (15) the heat source $H(r,t)$ becomes

$$\begin{aligned} H(r,t) &= H^{\mathrm{mod}}(r) H^{\mathrm{mod}}(t) \\ &= H^{\mathrm{mod}}(r)\big(A_0^{H,\mathrm{mod}} + A_{-1}^{H,\mathrm{mod}} e^{-i\omega_0 t} \\ &\quad + A_{+1}^{H,\mathrm{mod}} e^{i\omega_0 t}\big), \end{aligned} \tag{16}$$

where

$$H^{\mathrm{mod}}(r) = N_0\sigma \frac{E}{\tau_p} g(r), \tag{17}$$

and where the zero-th and first order Fourier coefficients of $H^{\mathrm{mod}}(t)$ are given by

$$A_0^{H,\mathrm{mod}} = \frac{1}{T}\int_0^{\tau_p} dt = \frac{\tau_p}{T}, \tag{18}$$

$$A_{\pm1}^{H,\mathrm{mod}} = \frac{1}{T}\int_0^{\tau_p} e^{\mp i\omega_0 t}\, dt = \frac{\pm i}{2\pi}\big[e^{\mp 2\pi i\, \tau_p/T} - 1\big]. \tag{19}$$

For a duty cycle $d$ of 50% ($\tau_p = d \cdot T$) the heat source is given by $H(r,t) = H^{\mathrm{mod}}(r)(\frac{1}{2} + \frac{2}{\pi}\sin(\omega_o t))$.

We denote by $S_n^{\mathrm{mod}}$ the magnitude of the PA signal in the modulated resonant case, which is given by $S_n^{\mathrm{mod}} = |A_{n,+1}| = |A_{n,-1}|$. From (8), (9), and (17) we can conclude that $S_n^{\mathrm{mod}}$ is proportional to the number density of absorbing species and the laser power. For a given output power $P$ of the laser ($E = d \cdot P \cdot T$), we can also show—using (8), (9), (17), and (19)—that the duty cycle for which $S_n^{\mathrm{mod}}$ is maximized is 50%.

#### 2.2.2 Pulsed resonant case

In the pulsed resonant case, the heat pulse generates an acoustic pulse that excites the eigenmodes of the resonator. The presented theory assumes that the acoustic pulse and the heat pulse have the same time profile. This condition may not be fulfilled in an actual experiment. A general theoretical treatment would go beyond the scope of this paper.

In the pulsed resonant case $\tau_p \ll \tau_{V-T}$. There is no significant vibrational–translational energy transfer during the pulse. Therefore, the term that accounts for collisional deactivation in (14) can be ignored during the pulse:

$$\frac{dN_1(r, t \le \tau_p)}{dt} = N_0\sigma\, \Phi(r,t). \tag{20}$$

With the help of (11) and (12) the above expression can be integrated over the duration of one pulse, which yields (assuming $N_1(r,0) = 0$)

$$N_1(r, t = \tau_p) = N_0\sigma \frac{E}{h\nu}\, g(r). \tag{21}$$

After the pulse, (14) can be written as

$$\frac{dN_1(r, t \gg \tau_p)}{dt} = -\frac{N_1(r,t)}{\tau_{V-T}}. \tag{22}$$

Taking the initial condition (21) into account, the solution of the above equation is

$$N_1(r, t \gg \tau_p) = N_0\sigma\, \frac{E}{h\nu}\, g(r)\, e^{\frac{-t}{\tau_{V-T}}}. \tag{23}$$

With (5), (13), and (23) the heat source $H(r,t)$ becomes

$$\begin{aligned} H(r,t) &= H^{\mathrm{pul}}(r) H^{\mathrm{pul}}(t) \\ &= H^{\mathrm{pul}}(r)\big(A_0^{H,\mathrm{pul}} + A_{-1}^{H,\mathrm{pul}} e^{-i\omega_0 t} + A_{+1}^{H,\mathrm{pul}} e^{i\omega_0 t}\big), \end{aligned} \tag{24}$$

where

$$H^{\mathrm{pul}}(r) = N_0\sigma \frac{E}{\tau_{V-T}} g(r), \tag{25}$$

and where the zero-th and first order Fourier coefficients of $H^{\mathrm{pul}}(t)$ are given by

$$A_0^{H,\mathrm{pul}} = \frac{1}{T}\int_0^{T} e^{\frac{-t}{\tau_{V-T}}}\, dt = \frac{1 - e^{\frac{-T}{\tau_{V-T}}}}{\frac{T}{\tau_{V-T}}}, \tag{26}$$

$$A_{\pm1}^{H,\mathrm{pul}} = \frac{1}{T}\int_0^{T} e^{\frac{-t}{\tau_{V-T}}}\, e^{\mp i\omega_0 t}\, dt = \frac{1 - e^{\frac{-T}{\tau_{V-T}}}}{\pm 2\pi i + \frac{T}{\tau_{V-T}}}. \tag{27}$$

We denote by $S_n^{\mathrm{pul}}$ the magnitude of the PA signal in the pulsed resonant case, which is given by $S_n^{\mathrm{pul}} = |A_{n,+1}| = |A_{n,-1}|$. From (8), (9), and (25) we can conclude that $S_n^{\mathrm{pul}}$ is proportional to the density of absorbing species and the average laser power.

### 2.3 Comparison between the modulated resonant and pulsed resonant cases

We assume that the pulse energy and the beam profile are the same in the modulated resonant and the pulsed resonant

cases. Furthermore, we assume a 50% duty cycle in the modulated resonant case. From (8), (9), (17), (19), (25), and (27) the PA signal ratio $R$ between both cases can be written as

$$R = \frac{S_n^{\mathrm{pul}}}{S_n^{\mathrm{mod}}} = \frac{|A_{+1}^{H,\mathrm{pul}} \int_V H^{\mathrm{pul}}(\mathbf{x})\, p_n(\mathbf{x})\, dV|}{|A_{+1}^{H,\mathrm{mod}} \int_V H^{\mathrm{mod}}(\mathbf{x})\, p_n(\mathbf{x})\, dV|}$$

$$= \frac{\alpha}{2} \frac{|A_{+1}^{H,\mathrm{pul}}|}{|A_{+1}^{H,\mathrm{mod}}|} = \frac{\pi}{2} \frac{1 - e^{-\alpha}}{\sqrt{1 + (2\pi/\alpha)^2}}, \tag{28}$$

where $\alpha = \frac{T}{\tau_{V-T}}$. Therefore, $R = \pi/2$ if $T \gg \tau_{V-T}$ as usually found in trace gas analyses.

## 3 Experimental setup

In order to compare the two modes of operation, two experimental setups, pictured in Figs. 1 and 2, were built using the same PA cell. A beam expanding telescope, placed before the PA cell, adjusted the beam diameter to about 1.3 mm. The wavelength (532 nm) was also the same in both cases. The PA cell, described previously [12], was mounted with four miniature microphones (Knowles Acoustics EK-3024) and a newly-designed microphone signal preamplifier. The cylindrical acoustic resonator of the PA cell was made of stainless steel. It had a length of 29 mm and a diameter of 6 mm. Nitrogen dioxide was supplied from a calibrated gas mixture (2000 ppmv $NO_2$ buffered in Ar) and was further diluted in argon by means of a mass flow controller to obtain the desired concentrations. A constant flow through the PA cell (typically 50 mL/min) was maintained during measurements to avoid adsorption effects [8]. The total pressure inside the PA cell was also maintained at 980 mbar. A lock-in amplifier read the pre-amplified microphone signal with a time constant of 1 s. A wedged window was placed after the PA cell. One of the beam reflections at the window interface was directed to a photodiode. The photodiode provided a reference signal, which was acquired by an oscilloscope. The reference signal was calibrated with a power meter to produce absolute values. Since the absorption in the cell was small, it did not influence the reference signal substantially. The lock-in and the oscilloscope acquisitions were synchronized. A LabVIEW program controlled the whole setup.

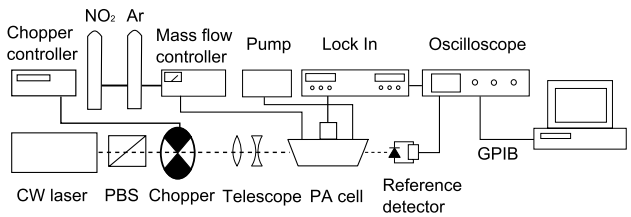


**Fig. 1** Experimental setup of the modulated resonant PA scheme

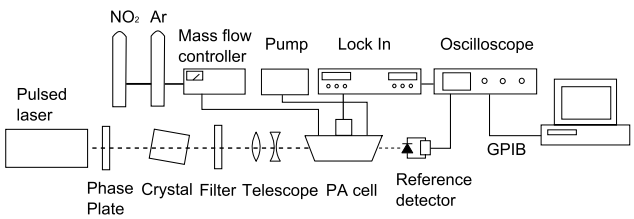


**Fig. 2** Experimental setup of the pulsed resonant PA scheme

### 3.1 Modulated resonant case

The optical source, pictured in Fig. 1, consisted in a cw intracavity-frequency-doubled diode-pumped Nd:YAG laser (CrystaLaser, Inc.) emitting at 532 nm. The laser source was modulated by a chopper up to a frequency of 6.4 kHz with a 50% duty cycle. The chopper controller provided a reference signal to the lock-in amplifier. The beam power was adjusted with a polarizing beam splitter (PBS). The PA signal was normalized with the photodiode signal.

### 3.2 Pulsed resonant case

The optical source, picture in Fig. 2, consisted in a Q-switched diode-pumped Nd:YAG laser (Innolight GmbH). The laser pulses were about 6 ns long. The pulse repetition rate was tunable between 4 and 7.5 kHz by changing the injection current of the pump diodes. Frequency-doubling took place in a type II non-critically phase-matched KTP crystal. The fundamental beam was filtered out after the KTP crystal. The laser power was adjusted by rotating a half-wave plate placed before the KTP crystal. The PA signal was normalized with the photodiode signal, which served as well as a reference to the lock-in amplifier.

## 4 Results and discussion

The PA resonance was measured using the modulated and pulsed optical arrangements. As pictured in Fig. 3, the resonance curves are in good agreement with each other. They are dominated by the first longitudinal acoustic mode, which is centered at 5.4 kHz as expected from theory taking argon as buffer gas into account [4]. Higher order resonator modes are expected above 30 kHz only. The $Q$-factor is 6.3 and 5.95 in the modulated and pulsed optical arrangement, respectively.

In a further series of measurements pictured in Figs. 4 and 5, we investigated the PA signal dependence on the $NO_2$ concentration and on the average laser power entering the cell. For each series, the repetition rate of the optical excitation was adjusted to the first longitudinal resonance

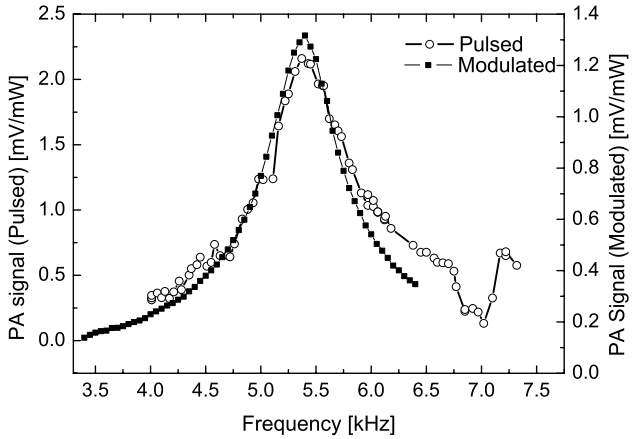


**Fig. 3** Resonance curve of the PA cell in the modulated and pulsed optical arrangements. Measurements were carried out with 2000 ppmv $NO_2$ diluted in argon at 980 mbar total pressure

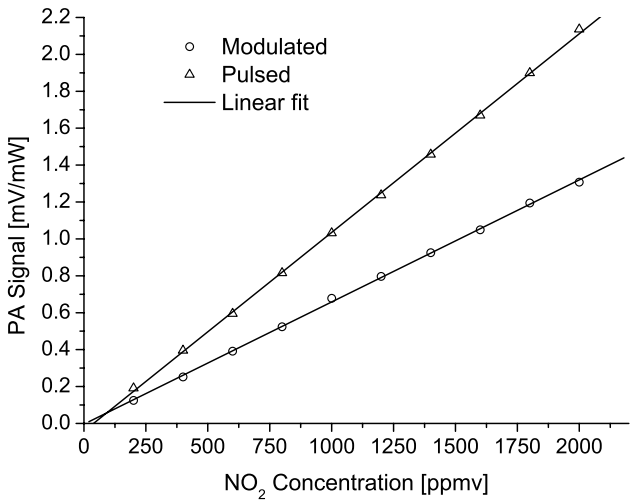


**Fig. 4** Dependence of the normalized PA signal on the $NO_2$ concentration in the modulated resonant and pulsed resonant cases. Measurements were carried out at a total pressure of 980 mbar

of the PA cell (5.4 kHz). As expected from Sects. 2.2.1 and 2.2.2, the PA signal increases linearly with respect to the $NO_2$ concentration and the average laser power. For a given $NO_2$ concentration inside the cell, the pulsed resonant PA signal is higher than the modulated PA signal by a factor $1.63 \pm 0.02$ (Fig. 4), whereas for a given average power of the laser this ratio is $1.95 \pm 0.03$ (Fig. 5). These results are in agreement with the model developed in Sect. 2, which predicts a factor $\pi/2 = 1.57$ (28). In the pulsed resonant PA scheme, the beam profile of the second harmonic was very sensitive to optical alignments and temperature variations of the KTP crystal. This could account for the small discrepancy between the theoretical PA signal ratio and the experimental ratio derived from Fig. 5.

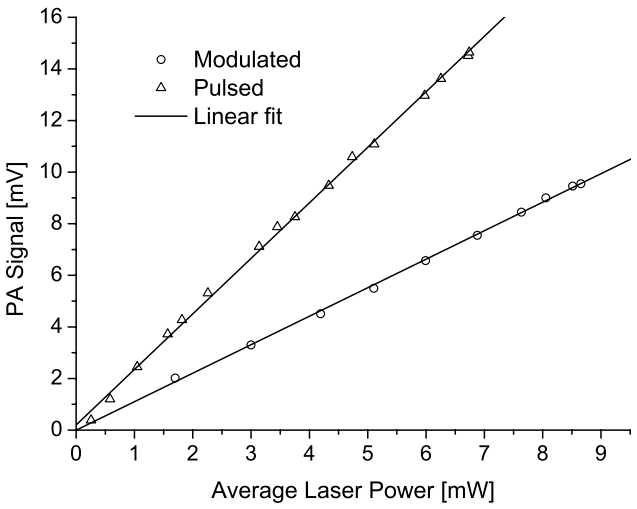


**Fig. 5** Dependence of the PA signal on the average laser power entering the PA cell. Measurements were carried out with 2000 ppmv $NO_2$ diluted in argon at 980 mbar total pressure. The modulated resonant case is compared to the pulsed resonant case

## 5 Conclusions

With respect to the modulated resonant scheme (optimized for a 50% duty cycle), pulsed resonant optical excitation produces $\pi/2$ times higher PA signals under similar experimental conditions, i.e. for the same average laser power and trace gas concentration. In both cases, the PA signal increases linearly with respect to the density of absorbing species and the average laser power as expected.

**Acknowledgements** M. Kaučikas acknowledges a fellowship granted by the Swiss Baltic Net program of the Gebert Rüf Stiftung. The authors would like to thank G. Poberaj for borrowing the cw laser source.

## References

1. M.W. Sigrist, *Air Monitoring by Spectroscopic Techniques*. Chemical Analysis Series, vol. 127 (Wiley, New York, 1994), pp. 163–238
2. F.J.M. Harren, G. Cotti, J. Oomens, S. te L. Hekkert, Photoacoustic spectroscopy in trace gas monitoring, in *Encyclopedia of Analytical Chemistry*, vol. 3, ed. by R.A. Meyers (Wiley, Chichester, 2000), pp. 2203–2226
3. M.W. Sigrist, R. Bartlome, D. Marinov, J.M. Rey, D.E. Vogler, H. Wachter, Trace gas monitoring with infrared laser-based detection schemes. Appl. Phys. B, Lasers Opt. **90**(2), 289–300 (2008)
4. A. Miklos, P. Hess, Z. Bozoki, Application of acoustic resonators in photoacoustic trace gas analysis and metrology. Rev. Sci. Instrum. **72**(4), 1937–1955 (2001)
5. S. Schafer, A. Miklos, P. Hess, Quantitative signal analysis in pulsed resonant photoacoustics. Appl. Opt. **36**(15), 3202–3211 (1997)
6. F.G.C. Bijnen, J. Reuss, F.J.M. Harren, Geometrical optimization of a longitudinal resonant photoacoustic cell for sensitive and fast trace gas detection. Rev. Sci. Instrum. **67**(8), 2914–2923 (1996)

7. C. Fischer, R. Bartlome, M.W. Sigrist, The potential of mid-infrared photoacoustic spectroscopy for the detection of various doping agents used by athletes. Appl. Phys. B, Lasers Opt. **85**(2–3), 289–294 (2006)
8. V. Slezak, J. Codnia, A.L. Peuriot, G. Santiago, Resonant photoacoustic detection of $NO_2$ traces with a q-switched green laser. Rev. Sci. Instrum. **74**(1), 516–518 (2003)
9. D. Costopoulos, A. Miklos, P. Hess, Detection of $N_2O$ by photoacoustic spectroscopy with a compact, pulsed optical parametric oscillator. Appl. Phys. B, Lasers Opt. **75**(2-3), 385–389 (2002)
10. J. Kalkman, H.W. Van Kesteren, Relaxation effects and high sensitivity photoacoustic detection of $NO_2$ with a blue laser diode. Appl. Phys. B, Lasers Opt. **90**(2), 197–200 (2008)
11. V. Slezak, High-precision pulsed photoacoustic spectroscopy in $NO_2$–$N_2$. Appl. Phys. B, Lasers Opt. **73**(7), 751–755 (2001)
12. C. Fischer, M.W. Sigrist, Q. Yu, M. Seiter, Photoacoustic monitoring of trace gases by use of a diode-based difference frequency laser source. Opt. Lett. **26**(20), 1609–1611 (2001)